Denoyer, L., Benavidez, A., Brearley, A., Ramaiyan, K. and Garzon, F. (2023) Chemical stabilit
y of BaMg0.33Nb0.67-xFexO3-δ in high-temperature methane conversion environments.
ECS Trans. 111 587. https://doi 10.1149/11106.0587ecst

Chemical Stability of $BaMg_{0.33}Nb_{0.67-X}Fe_xO_{3-\delta}$ in High Temperature Methane Conversion Environments

L. H. Denoyer, A. Benavidez, A. Brearley, K. P. Ramaiyan*, F. H. Garzon*

Chemical and Biological Engineering Department, Center for Micro-Engineered Materials, University of New Mexico, Albuquerque, NM 87131, USA.

Doped perovskite metal oxide catalysts of the form $A(B_xM_{1-x})O_{3-\delta}$ have been instrumental in the development of solid oxide electrolyzers/fuel cells. In addition, this material class has also been demonstrated to be effective as a heterogeneous catalyst. Co-doped barium niobate perovskites have shown remarkable stability in highly acidic CO_2 sensing measurements/environments (1). However, the reason for their chemical stability is not well understood. Doping with transition metal cations for B site cations often leads to exsolution under reducing conditions. Many perovskites used for the oxidative coupling of methane (OCM) or the electrochemical oxidative coupling of methane (E-OCM) either lack long term stability, or catalytic activity within these highly reducing methane environments. The Mg and Fe co-doped barium niobate $BaMg_{0.33}Nb_{0.67-x}Fe_xO_{3-\delta}$ shown activity in E-OCM reactors over long periods (2) (>100 hrs) with no iron metal exsolution observed by diffraction or STEM EDX measurements. In contrast, iron decorated $BaMg_{0.33}Nb_{0.67}O_3$ showed little C2 conversion activity.

Introduction

The ability to engineer perovskites with nonstoichiometric A and B sites of the form - $A_{1-x}A'_xB_{1-y}B'_yO_{3\pm\delta}$, allow for fine tuning of electronic properties (3) (also viable for perovskite solar cells (4) and oxygen vacancy formation (5) within perovskite lattice structures. An increase in oxygen vacancies within perovskite lattices allows for higher oxygen anion mobility and electrocatalytic effects as seen with surface oxygen mobility for O^-/O^{2-} in OCM reaction (6).This article focuses on the stability of co-doped barium niobate perovskites in high concentration methane environments, which simulate conditions for the anode in the electrochemical oxidative coupling of methane (E-OCM) where the desired product is ethylene or ethane.

$Sr_2Fe_{1.5+0.075}Mo_{0.5}O_{6-\delta}$ (SFMO-075Fe) was previously reported to convert CH_4 to C_2 products with a Faradaic efficiency of 82% (7). However, our group has shown that under long temperature holds with methane environments (>95% CH_4 at minimum) $Sr_2Fe_{1.5+}Mo_{0.5}O_{6-\delta}$ and $Sr_2Fe_{1.5+0.075}Mo_{0.5}O_{6-\delta}$ materials lose crystallinity and are also susceptible to both coke and carbonate formation (8). Thus, here we explored the use of a perovskite material previously demonstrated to be stable for CO_2 gas sensing applications, $BaMg_{0.33}Nb_{0.67-x}Fe_xO_{3-\delta}$ (BMNF) (1). When using BMNF as an anode for E-OCM, we found that this material is both capable of converting methane into ethylene products (at

cell voltages >0V versus air) and withstanding high temperature holds at temperatures up to 900 °C for over 100 hours without coking or structural collapse (2). Therefore, this article aims to explore how this class of perovskites at lower doping levels maintains stability in methane environments, via temperature programmed reaction (TPR) measurements, as well as further property modifications via doping or by decorating the parent barium magnesium niobate with Fe nanoparticles.

Experimental methods

Sample synthesis

$BaMg_{0.33}Nb_{0.67-x}Fe_xO_{3-\delta}$ was prepared via traditional solid-state synthesis using oxide and carbonate precursors, with x = 0, 0.17, 0.25 and 0.33 (Hereafter referred to as BMN, BMNF17, BMNF25, and BMNF33. Our previous study reported on the redox stability of BMNF33 materials, however some second phases were present in the sample and the 900 °C used in the study tends to promote homogenous reactions of methane. Additionally, a BMN sample with 0.1 moles stoichiometric Fe added (BMN+01Fe) via an incipient wetness impregnation synthesis method was prepared to evaluate whether low concentration of surface iron is detectable by X-ray diffraction (XRD) and to contrast the catalytic behavior of iron decorated BMN with the BMNF samples.

Sample characterization

XRD scans were taken with a PANalytical X'Pert Pro diffractometer with a sealed Cu-$K\alpha_{1,2}$ radiation, X-ray source, 45 kV and 40mA, Goebel Mirror Monochromator, Bragg-Brentano geometry, in air from 5-105° (2- theta) and a 1-D PIXcel strip detector. Powder samples were placed on zero-background quartz slides and dried in isopropyl alcohol or acetone before measurements. Individual scans were run for 13 minutes. Whole Pattern Fitting (WPF) of the perovskite oxide sample data was performed using Rietveld refinement analysis techniques, MDI Jade 9 software. A $Ba(Mg_{0.33}Nb_{0.667})O_{3-\delta}$, ICDD card PDF#04-015-0842, was used for the base starting fitting profile parameters. XRD was performed on all the as prepared compositions from BMNF17-33 as well as on the incipient wetness prepared BMN-01Fe.

Reaction conditions

Temperature programmed reaction measurements utilizing a programmable tube furnace were carried out to evaluate the chemical stability of these materials. The exit gas was analyzed using a MKS Cirrus Mark II mass spectrometer and an SRI 8610C Gas Chromatograph. During TPR the following conditions were used: 95% CH_4 and 5% O_2 at a volumetric flow of 25 SCCM; 5 °C/min temperature ramp and 2-hour hold at 800 °C. A tubular reactor setup is used with 15mm inner diameter alumina tubing. Quartz wool was packed on both sides of the sample to create a catalyst bed and prevent samples from displacement within the reactor hot zone. 100 mg of extra course silicon carbide granules were used to limit sample powders from sintering together within the reactor bed. TPR experiments using only the silicon carbide granules were performed to establish a baseline. No significant methane to C2 conversion was observed over SiC. 50 mg of perovskite sample was used for testing unless otherwise specified.

Results and Discussion

X-ray diffraction

Powder X-ray diffraction scans were taken of the samples both directly after synthesis (final sintering at 1400 °C) and after exposure to 95% CH_4 and 5% O_2 as seen in TPR measurement. As shown in Figure 1a and Figure 1c, both the before and after TPR BMNF materials are well-formed, single perovskites with little to no change in crystalline structure. As seen in BMNF17 and BMNF25, there were no peaks detected for secondary phase material, which was not the case for BMNF33 (highest iron doping). After performing whole pattern fitting and structure refinement with MDI Jade 9 and the accompanying PDF card (PDF#04-015-0842), the BMNF materials were fit to $BaMg_{0.33}Nb_{0.67}O_{3-\delta}$ structure. The Pm3m space group of the reference structure was used for fitting, this gave an $R \approx 10\%$ and $E < 10\%$, indicating there is no significant difference in the structures of doped BMN structure and BMNF structures and no prominent secondary phases were observed in BMNF17 and BMNF25. The BMNF samples generally show very slight peak shifts away from BMN primary peak position (011) shown in Figure 1b. The X-ray unit cell lattice parameters were also refined using a WPF. Both lattice constants for the materials in Figure 1 and the crystallite size are listed in Table 1. The cell constant shift for BMNF17, BMNF25 and BMNF33, observed through WPF, indicate a very slight unit cell contraction ~0.01Å upon iron doping of the BNM structure. The crystallite size also increases in the BMNF25/33 materials, indicative of enhanced particle sintering/grain growth in the presence of iron doping. The lack of second phase formation in BMNF17 and BMNF25 also indicate an Fe solubility limit that has not been previously reported. Future XAS and neutron diffraction studies are planned to determine the effects of iron on bond length and oxygen vacancy formation in doped $BaNbO_3$ materials.

TABLE I. Lattice constants and crystallite size from PXRD

Sample Name	Lattice Constant (Å)	Crystallite Size (Å)	R (%)	E (%)
BMN	4.0910	37.22	11.61	9.98
BMNF17	4.0814	38.88	10.37	7.87
BMNF25	4.0694	66.95	9.05	7.62
BMNF33	4.0804	52.22	15.80	14.18
BMN TPR	4.0906	53.42	14.15	11.88
BMNF17 TPR	4.0815	50.80	13.01	10.96
BMNF25 TPR	4.0749	56.66	12.80	11.34
BMNF33 TPR	4.0788	75.14	13.61	11.75

Near peak position $2\theta = 28°$ in Figure 1c, there are no new peak formations for any BMNF sample other than BMNF33. The BMNF33 may have reached its saturation limit for iron, therefore unable to accommodate more Fe into B site lattice positions. As seen previously, there may be also tendency towards exsolution with perovskite materials that have slightly higher nonstoichiometric iron loading with otherwise stable structures(8–11). This effect is clearly seen in Figure 1c, where there appears to be new peak formations for BMNF33, indicative of a second phase formation. Further explanation of the effects this may have on heterogenous reaction will be discussed in the temperature programmed reaction section. Figure 1d illustrates slight shifts in the primary peak positions, as visual evidence of the similarities between the BMNF samples maintaining similar crystal structures both before and after TPR treatment. The BMNF samples are otherwise stable

under hydrogen and methane reducing conditions. The overall crystal lattice with incorporated iron maintains a nearly similar lattice constant and unit cell crystal size to the BMN material. PXRD scans of BMN+01Fe show no indication of Fe species, with the pattern appearing nearly identical to the as prepared BMN samples. The PXRD technique is however limited in sensitivity to detect low concentrations of nanoclusters.

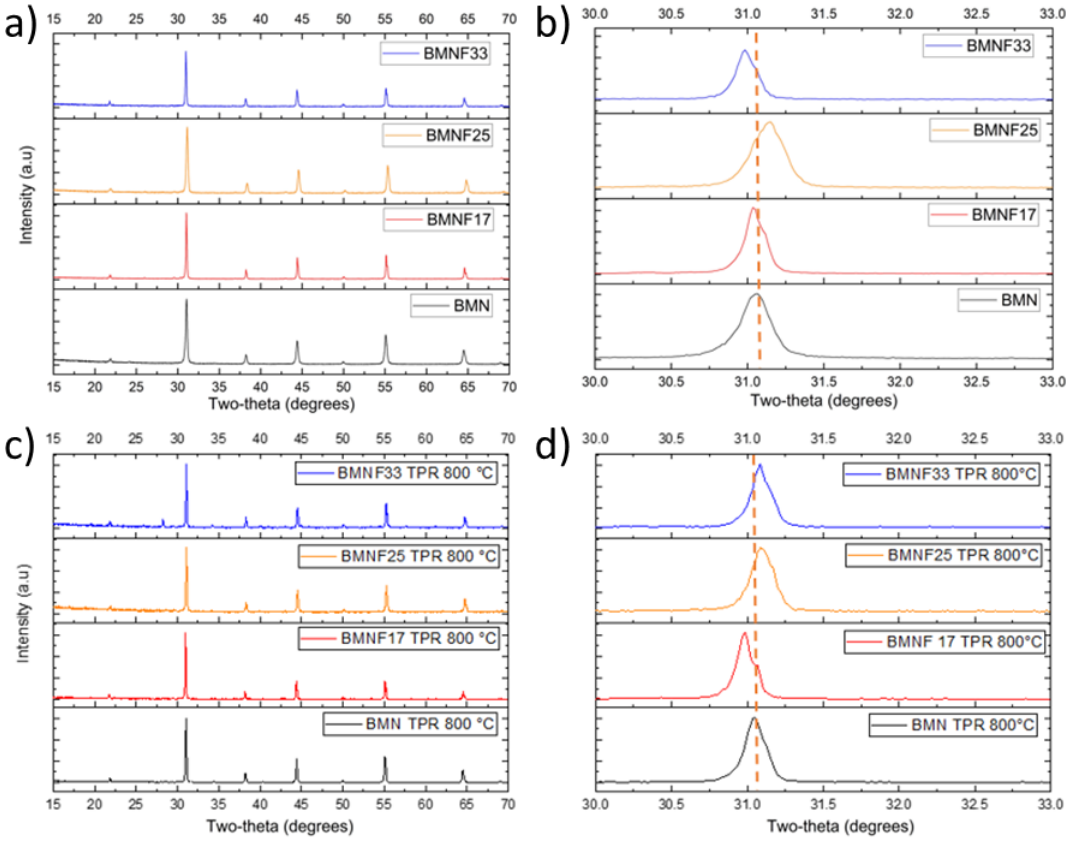

Figure 1. Powder X-ray diffraction (PXRD) taken for (a) As prepared powders, (b) zoomed in 100% intensity peak on crystal plane (011) for BMN series (c) BMNF samples after temperature programmed reduction treatment and (d) BMNF powder diffraction scan enlarged at around 31.5° 2-theta angle.

Temperature programmed reaction and STEM analysis

Temperature programmed reactions were conducted with all listed materials in Table 1 as well as with BMN+01Fe. Included in Figure 2 are two samples. Figure 2a features BMN, $BaMg_{0.33}Nb_{0.67}O_{3-\delta}$ without any Fe, to test the reactivity of the perovskite. Previously, it was found that the conductivity of these BMNF materials was greatly enhanced by the addition of Fe(2). The BMN material has a conductivity <<1 mS/cm, making it effectively an insulator at these reaction conditions. This limits the possibility of oxide ion/electron transport and diminishes its feasibility as an alternative anode material for E-OCM. As seen in Figure 2a, the primary product for BMN is CO_2, at roughly 6.5 relative concentration ratio of C_2H_4 being generated. The yield for C_2H_4 is more than doubled for BMNF25 which is shown in Figure 2b. The onset temperature of reactant feed conversion is also much sooner than in BMN. This indicates that addition of Fe into the

BMNF structure not only increases selectivity towards C_2H_4, but also lowers activation energy for reaction. In contrast the BMN+01Fe sample showed little selectivity towards ethylene formation and favored CO and H_2 products (H_2O is pre-condensed and not detectable) as shown in Figure 2c. Due to complexity of these reaction mechanisms, further TPR studies at varying gas compositions and temperatures are required to elucidate the reaction pathways.

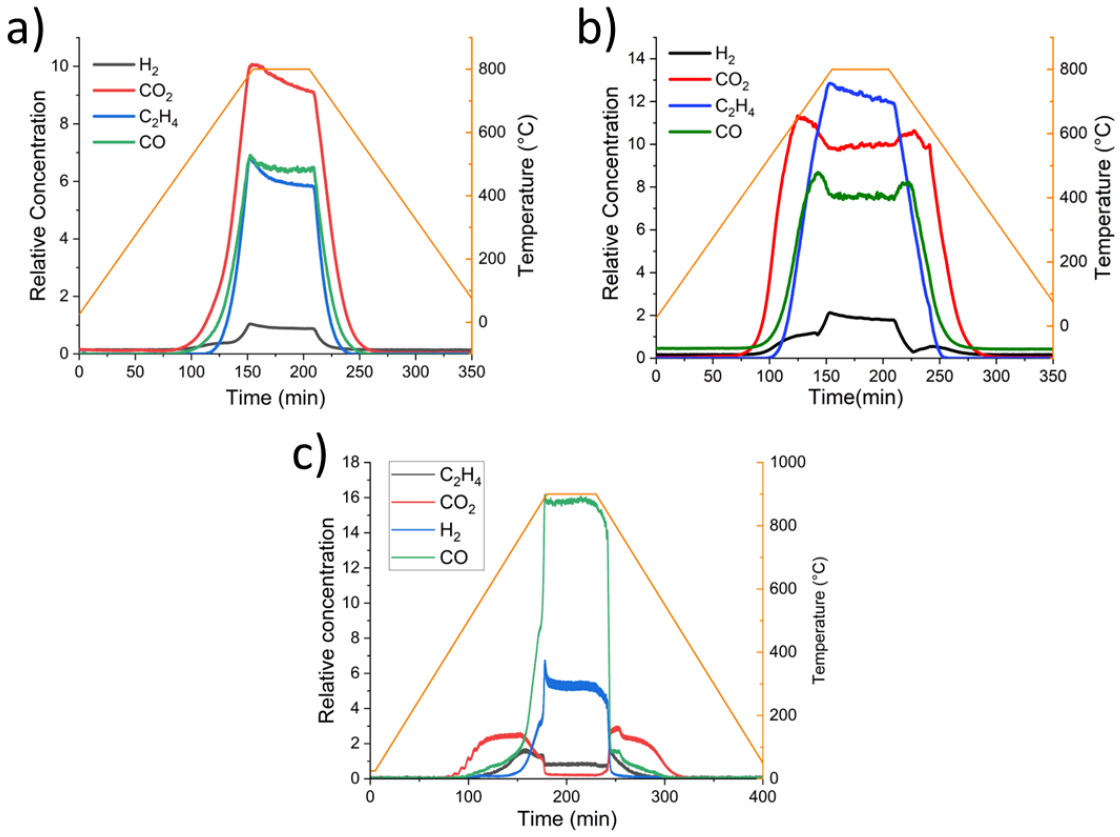

Figure 2. Temperature programmed reaction for (a) BMN without any iron, (b) BMNF25 in which the temperature of reaction was held at 800 °C, and (c) BMN+01Fe in which the temperature of reaction was held at 900 °C. Note that reaction conditions are the same for all samples other than c (temperature hold at 900 °C).

STEM and EDX measurements were taken on the 200 KeV aberration corrected JEOL NEOARM STEM microscope at the University of New Mexico. The goal was to examine the BMNF25 material prepared from solid state synthesis and identify any possible changes in atomic distribution of Fe, which has previously been observed in other perovskite materials(12). Results from STEM studies indicate crystallite formation with particle sizes variances in size and distribution, clearly polycrystalline in nature for both BMN+01Fe and BMNF25 as shown in Figure 3. EDX mapping was used to determine the elemental spatial distribution for both the Fe and Nb species.

The BMN+01Fe material in Figure 3a illustrates a relatively uniform distribution of Fe and Nb, showing that the additional Fe is well dispersed on the surface, with little evidence of clustering or nanoparticle formation. Figure 3d also illustrates pristine

BMNF25 after preparation, with EDX spectra of Fe and Nb. These spectra are taken for Ba and Mg species, although not shown here. As seen in Figure 3b, the BMN+01Fe sample after H_2 treatment shows evidence of nanoparticle formation. BMN+01Fe treated in CH_4 also show particle agglomeration for Fe on the surface. However, this phenomenon is not seen in Figure 3e and 3f; BMNF25 samples after H_2 treatment and methane treatment. These samples were treated in H_2 (Figures 3b/e) and CH_4 (Figures 3c/f) at 800 °C for 4 hours each. The overall nanoparticle size and composition is not easily seen at this magnification, however Figure 3e and 3f illustrate that the BMNF25 structure roughly maintains the same Fe concentration both before and after gas treatment, indicative of a very stable crystalline lattice that is averse to B site cation migration via reduction. Experimental STEM sample preparation challenges have precluded high resolution imaging of our anodes from our electrochemical partial oxidation experiments, where effects of electric potentials and ion transport may promote iron segregation. However, our previous electrochemical testing has shown BMNF25 to be stable and responsive to voltage after high temperature holds.(2) This may indicate that Fe sites on the surface of BMNF25 are not poisoned or formed into Fe nanoclusters, which would affect the activity of the partial oxidation catalyst.

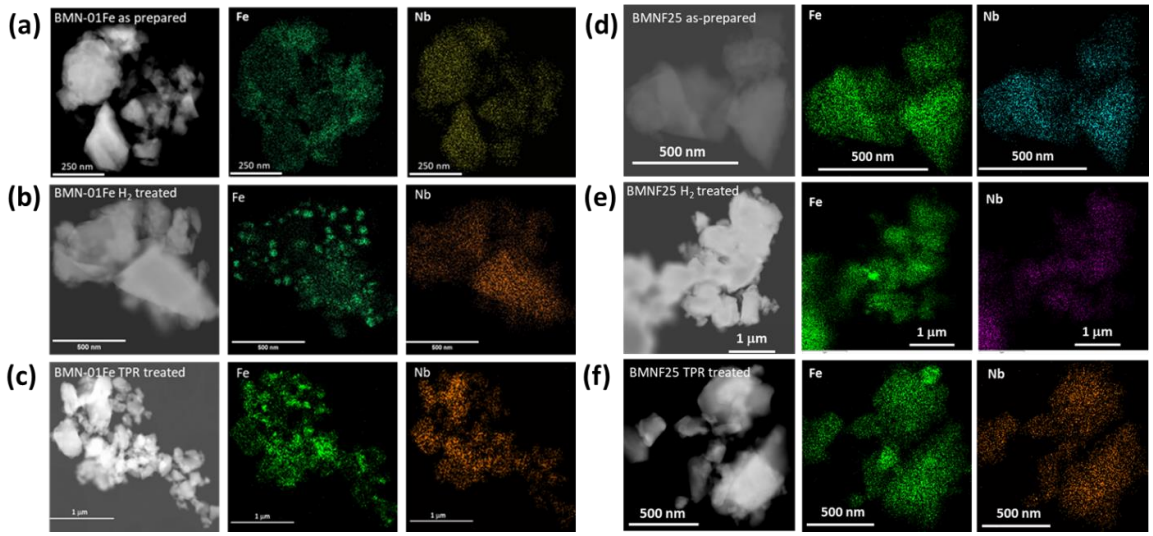

Figure 3. STEM and EDX maps showing the elemental distribution of Fe and Nb for the BMN-01Fe powder (a) as prepared, (b) after H_2 treatment, (c) after TPR measurements and that of BMNF25 (d) as prepared, (e) after H_2 treatment, (f) after TPR measurements.

Conclusions

The $BaMg_{0.33}Nb_{0.67-x}Fe_xO_{3-\delta}$ (BMNF) materials were shown to be stable in reducing methane conversion environments. This is in contrast to many Fe containing perovskites that exsolve under reducing conditions. Incorporation of Fe into the host perovskite lattice beneficially affects ethylene yield during heterogenous OCM measurements, thus indicating that these materials can be utilized in a variety of applications in both electrochemical and catalytic settings. Through XRD, STEM and TPR characterization and heterogeneous catalysis experimentation, insights were discovered about the role of Fe substitution into BMN as well as structural characteristics that may lead to descriptors for successful E-OCM anodes in the future. While transition metal exsolution from perovskite

structures is generally favorable for promoting complete hydrocarbon oxidation, it appears that partial oxidation is best promoted by ionic iron within the perovskite lattice.

Acknowledgments

The authors thank the NSF – Center for Innovative and Strategic Transformation of Light Alkane Resources (CISTAR) (NSF – CISTAR Award No. EEC-1647722) for funding this work.

References

1. Kannan R, Mulmi S, Thangadurai V. 2013. Synthesis and characterization of perovskite-type BaMg0.33Nb0.67−xFexO3−δ for potential high temperature CO2 sensors application. *J. Mater. Chem. A*. 1(23):6874–79
2. Denoyer LH, Benavidez A, Garzon FH, Ramaiyan KP. 2022. Highly Stable Doped Barium Niobate Based Electrocatalysts for Effective Electrochemical Coupling of Methane to Ethylene. *Adv. Mater. Interfaces*. 9(27):2200796
3. Hasan M, Nasrin S, Islam MN, Hossain AKMA. 2022. First-principles insights into the electronic, optical, mechanical, and thermodynamic properties of lead-free cubic ABO3 [A = Ba, Ca, Sr; B = Ce, Ti, Zr] perovskites. *AIP Adv.* 12(8):085327
4. Senocrate A, Spanopoulos I, Zibouche N, Maier J, Islam MS, Kanatzidis MG. 2021. Tuning Ionic and Electronic Conductivities in the "Hollow" Perovskite {en}MAPbI3. *Chem. Mater.* 33(2):719–26
5. Ji Q, Bi L, Zhang J, Cao H, Zhao XS. 2020. The role of oxygen vacancies of ABO3 perovskite oxides in the oxygen reduction reaction. *Energy Environ. Sci.* 13(5):1408–28
6. Sato A, Ogo S, Takeno Y, Takise K, Seo JG, Sekine Y. 2019. Electric Field and Mobile Oxygen Promote Low-Temperature Oxidative Coupling of Methane over La1–xCaxAlO3−δ Perovskite Catalysts. *ACS Omega*. 4(6):10438–43

7. Zhu C, Hou S, Hu X, Lu J, Chen F, Xie K. 2019. Electrochemical conversion of methane to ethylene in a solid oxide electrolyzer. *Nat. Commun.* 10(1):1173
8. Ramaiyan KP, Denoyer LH, Benavidez A, Garzon FH. 2021. Selective electrochemical oxidative coupling of methane mediated by Sr2Fe1.5Mo0.5O6-δ and its chemical stability. *Commun. Chem.* 4(1):1–9
9. Islam QA, Paydar S, Akbar N, Zhu B, Wu Y. 2021. Nanoparticle exsolution in perovskite oxide and its sustainable electrochemical energy systems. *J. Power Sources*. 492:229626
10. Kim YH, Jeong H, Won B-R, Myung J. Exsolution Modeling and Control to Improve the Catalytic Activity of Nanostructured Electrodes. *Adv. Mater.* n/a(n/a):2208984
11. Meng X, Wang Y, Zhao Y, Zhang T, Yu N, et al. 2020. In-situ exsolution of nanoparticles from Ni substituted Sr2Fe1.5Mo0.5O6 perovskite oxides with different Ni doping contents. *Electrochimica Acta*. 348:136351
12. Sinmyo R, Hirose K, Nishio-Hamane D, Seto Y, Fujino K, et al. 2008. Partitioning of iron between perovskite/postperovskite and ferropericlase in the lower mantle. *J. Geophys. Res. Solid Earth*. 113(B11):